Published in final edited form as:
Bioconjug Chem. 2009 April ; 20(4): 750–759. doi:10.1021/bc800455p.

Improving Tumor Uptake and Pharmacokinetics of ^{64}Cu-Labeled Cyclic RGD Peptide Dimers with Gly_3 and PEG_4 Linkers

Jiyun Shi[1], **Young-Seung Kim**[1], **Shizhen Zhai**[1], **Zhaofei Liu**[2], **Xiaoyuan Chen**[2], and **Shuang Liu**[1,*]

1*School of Health Sciences, Purdue University, West Lafayette, IN 47907, USA*

2*Molecular Imaging Program at Stanford (MIPS), Department of Radiology & Bio-X, Stanford University, Stanford, CA 94305-5484, USA*

Abstract

Radiolabeled cyclic RGD (Arg-Gly-Asp) peptides represent a new class of radiotracers with potential for the early tumor detection and non-invasive monitoring of tumor metastasis and therapeutic response in cancer patients. This report describes the synthesis of two cyclic RGD peptide dimer conjugates, DOTA-PEG_4-E[PEG_4-c(RGDfK)]$_2$ (DOTA-3PEG_4-dimer: DOTA = 1,4,7,10-tetraazacyclododecane-1,4,7,10-tetraacetic acid; PEG_4 = 15-amino-4,7,10,13-tetraoxapentadecanoic acid) and DOTA-G_3-E[G_3-c(RGDfK)]$_2$ (DOTA-3G_3-dimer: G_3 = Gly-Gly-Gly). Integrin $\alpha_v\beta_3$ binding affinities of cyclic RGD peptides were determined by competitive displacement of ^{125}I-echistatin bound to U87MG human glioma cells, and follow the order of DOTA-E{E[c(RGDfK)]$_2$}$_2$ (DOTA-tetramer: IC_{50} = 10 ± 2 nM) > DOTA-3G_3-dimer (IC_{50} = 62 ± 6 nM) ~ DOTA-3PEG_4-dimer (IC_{50} = 74 ± 3 nM) > DOTA-E[c(RGDfK)]$_2$ (DOTA-dimer: IC_{50} = 102 ± 5 nM). The addition of PEG_4 and G_3 linkers between two cyclic RGD motifs in DOTA-3G_3-dimer and DOTA-3PEG_4-dimer makes it possible for them to achieve the simultaneous integrin $\alpha_v\beta_3$ binding in a bivalent fashion. Both ^{64}Cu(DOTA-3PEG_4-dimer) and ^{64}Cu(DOTA-3G_3-dimer) were prepared in high yield with specific activity being >50 Ci/mmol. Biodistribution and imaging studies were performed in athymic nude mice bearing U87MG human glioma xenografts. The results from those studies show that PEG_4 and G_3 linkers are particularly useful for improving tumor uptake and clearance kinetics of ^{64}Cu radiotracers from the non-tumor organs, such as kidneys, liver and lungs. There is a linear relationship between the tumor size and %ID tumor uptake, suggesting that ^{64}Cu(DOTA-3PEG_4-dimer) and ^{64}Cu(DOTA-3PEG_4-dimer) might be useful for noninvasive monitoring of tumor growth or shrinkage during anti-angiogenic therapy. MicroPET imaging data clearly demonstrate the utility of ^{64}Cu(DOTA-3G_3-dimer) as a new PET radiotracer for imaging integrin $\alpha_v\beta_3$-positive tumors.

Keywords

integrin $\alpha_v\beta_3$; ^{64}Cu-labeled cyclic RGD peptides; PET tumor imaging

INTRODUCTION

Angiogenesis is a requirement for tumor growth and metastasis (1-10). Without neovasculature to provide oxygen and nutrients, tumors cannot grow beyond 1 - 2 mm in size. Once vascularized, previously dormant tumors begin to grow rapidly and their volumes increase

*To whom correspondence should be addressed: School of Health Sciences, Purdue University, 550 Stadium Mall Drive, West Lafayette, IN 47907. Phone: 765-494-0236; Fax 765-496-1377; Email: E-mail: lius@pharmacy.purdue.edu.

exponentially. Recent clinical and experimental evidence suggests that the tumor growth and progression are dependent on angiogenesis and invasion, which share common regulatory mechanisms (2,5). Angiogenesis is an invasive process characterized by endothelial cell proliferation, and is regulated by cell adhesion receptors. Integrins are such a family of proteins that facilitate cellular adhesion to and migration on extracellular matrix proteins found in intercellular spaces and basement membranes, and regulate cellular entry and withdraw from the cell cycle (5-13). Integrin $\alpha_v\beta_3$ is a receptor for the extracellular matrix proteins with exposed arginine-glycine-aspartic (RGD) tripeptide sequence (5,6,9). Integrin $\alpha_v\beta_3$ is normally expressed at low levels on epithelial cells and mature endothelial cells; but it is highly expressed on the activated endothelial cells in the neovasculature of tumors, including osteosarcomas, glioblastomas, melanomas, lung carcinomas, and breast cancer (11-19). It has demonstrated that integrin $\alpha_v\beta_3$ is overexpressed on both endothelial and tumor cells in human breast cancer xenografts (20). The integrin $\alpha_v\beta_3$ expression correlates well with tumor progression and invasiveness of melanoma, glioma and breast cancers (13-16,18-20). The highly restricted expression of integrin $\alpha_v\beta_3$ during tumor growth, invasion and metastasis presents an interesting molecular target for early detection of rapidly growing and metastatic tumors (21-33). In addition, it would be highly advantageous to develop an integrin $\alpha_v\beta_3$-specific radiotracer that could be used to non-invasively visualize and quantify the integrin $\alpha_v\beta_3$ expression level before, during or after antiangiogenic therapy (34).

Over the last several years, many radiolabeled cyclic RGD peptides have been evaluated as potential radiotracers for imaging the integrin $\alpha_v\beta_3$-positive tumors by single photon emission computed tomography (SPECT) or positron emission tomography (PET) (35-68). The integrin $\alpha_v\beta_3$-targeted radiotracers have recently been reviewed extensively (21-33). Among the radiotracers evaluated in different pre-clinical tumor-bearing animal models, [^{18}F]-AH111585, the core peptide sequence originally discovered from a phage display library (such as ACDRGDCFCG), and [^{18}F]Galacto-RGD (2-[^{18}F]fluoropropanamide c(RGDfK(SAA); SAA = 7-amino-L-glyero-L-galacto-2,6-anhydro-7-deoxyheptanamide) are under clinical investigations for noninvasive visualization of integrin $\alpha_v\beta_3$ expression in cancer patients (69-71). The imaging studies in cancer patients show that the ^{18}F-labeled cyclic RGD peptides are able to target the integrin $\alpha_v\beta_3$-positive tumors. However, the low tumor uptake, high cost and lack of preparation modules for the ^{18}F-labeled monomeric cyclic RGD peptides impose a significant challenge for their continued clinical applications.

To improve the integrin $\alpha_v\beta_3$ binding, multimeric cyclic RGD peptides, such as E[c(RGDfK)]$_2$ (dimer) and E{E[c(RGDfK)]$_2$}$_2$ (tetramer), were used as targeting biomolecules to carry radionuclide (e.g. ^{99m}Tc, ^{18}F, ^{64}Cu, and ^{111}In) to the integrin $\alpha_v\beta_3$ on tumor cells and endothelial cells of the tumor neovasculature (41-43,47-68). The results from the in vitro assays, ex-vivo biodistribution and in vivo imaging studies clearly demonstrate that the radiolabeled (^{99m}Tc, ^{18}F, ^{64}Cu, and ^{111}In) multimeric cyclic RGD peptides, such as E{E[c(RGDxK)]$_2$}$_2$ and E[c(RGDxK)]$_2$ (x = f and y), have much better tumor targeting capability as evidenced by their higher tumor uptake with longer tumor retention times as compared to their monomeric RGD peptide counterparts (47-68). However, it remains unclear if the cyclic RGD motifs in E{E[c(RGDxK)]$_2$}$_2$ and E[c(RGDxK)]$_2$ (x = f and y) are indeed able to achieve simultaneous integrin $\alpha_v\beta_3$ binding in a bivalent fashion. In addition, the uptake of the radiolabeled (^{99m}Tc, ^{18}F, ^{64}Cu and ^{111}In) multimeric cyclic RGD peptides in the kidneys and liver is also increased as the peptide multiplicity increases (51-54,60-68).

We recently reported the evaluation of two ^{99m}Tc-labeled cyclic RGD dimers, [^{99m}Tc(HYNIC-3PEG$_4$-dimer)(tricine)(TPPTS)] (^{99m}Tc-3PEG$_4$-dimer: HYNIC = 6-hydrazinonicotinyl, 3PEG$_4$-dimer = PEG$_4$-E[PEG$_4$-c(RGDfK)]$_2$, PEG$_4$ = 15-amino-4,7,10,13-tetraoxapentadecanoic acid, and TPPTS = trisodium triphenylphosphine-3,3',3''-trisulfonate) and [^{99m}Tc(HYNIC-3G$_3$-dimer)(tricine)(TPPTS)] (^{99m}Tc-3G$_3$-dimer: 3G$_3$-

dimer = G_3-E[G_3-c(RGDfK)]$_2$ and G_3 = Gly-Gly-Gly), as new radiotracers for imaging integrin $\alpha_v\beta_3$ expression in the athymic nude mice bearing U87MG glioma and MDA-MB-435 breast cancer xenografts (72,73). The PEG_4 and G_3 linkers are used to increase the distance between two cyclic RGDfK motifs from 6 bonds (excluding side arms of K-residues) in E[c(RGDfK)]$_2$ to 26 bonds in $3G_3$-dimer and 38 bonds in $3PEG_4$-dimer so that they are able to achieve simultaneous integrin $\alpha_v\beta_3$ binding in a bivalent fashion, and to improve the radiotracer excretion kinetics from non-cancerous organs. Results from the $\alpha_v\beta_3$ integrin binding assay show that the addition of two PEG_4 or G_3 linkers between two cyclic RGD motifs makes $3PEG_4$-dimer and $3G_3$-dimer bivalent in binding to the integrin $\alpha_v\beta_3$. The results from ex-vivo biodistribution studies clearly demonstrate that PEG_4 and G_3 linkers are useful for improving the tumor uptake and clearance of ^{99m}Tc-$3PEG_4$-dimer and ^{99m}Tc-$3G_3$-dimer from kidneys and liver. These promising results led us to prepare DOTA-$3PEG_4$-dimer and DOTA-$3G_3$-dimer (DOTA = 1,4,7,10-tetraazacyclododecane-1,4,7,10-tetraacetic acid), and their corresponding ^{64}Cu complexes, ^{64}Cu(DOTA-$3PEG_4$-dimer) and ^{64}Cu(DOTA-$3G_3$-dimer).

In this report, we present the synthesis and evaluation of ^{64}Cu(DOTA-$3PEG_4$-dimer) and ^{64}Cu(DOTA-$3G_3$-dimer) as PET radiotracers for imaging integrin $\alpha_v\beta_3$ expression in athymic nude mice bearing the U87MG glioma xenografts. We are particularly interested in ^{64}Cu because of its longer half-life ($t_{1/2}$= 12.7 h) than ^{18}F ($t_{1/2}$= 110 min). ^{64}Cu decays by β^+ emission (18% abundance, maximum β^+ energy of 0.655 MeV). It can be produced with high specific activity (74). All these factors make the ^{64}Cu-labeled cyclic RGD peptides very attractive as PET radiotracers. DOTA was chosen because it forms a highly stable ^{64}Cu chelate (75-77). The main objective of this study is to assess the impact of PEG_4 and G3 linkers on integrin $\alpha_v\beta_3$ binding affinity of DOTA-conjugated cyclic RGD peptide dimers, and on the tumor uptake and excretion kinetics of their ^{64}Cu radiotracers from noncancerous organs, particularly the kidneys and liver. The results from the integrin $\alpha_v\beta_3$ binding assay and biodistribution studies may also allow us to compare them with ^{64}Cu(DOTA-dimer) and ^{64}Cu(DOTA-tetramer).

EXPERIMENTAL SECTION

Materials

Chemicals were purchased from *Sigma-Aldrich* (St. Louis, MO). DOTA-NHS (1,4,7,10-tetraazacyclododecane-1-(N-hydroxysuccinimide acetate)-4,7,10-triacetic acid) was obtained from Macrocyclics Inc. (Dallas, TX). Peptide dimers, PEG_4-E[PEG_4-c(RGDfK)]$_2$ ($3PEG_4$-dimer) and G_3-E[G_3-c(RGDfK)]$_2$ ($3G_3$-dimer), were custom-made by Peptides International, Inc. (Louisville, KY). The ESI (electrospray ionization) mass spectral data were collected on a Finnigan LCQ classic mass spectrometer, School of Pharmacy, Purdue University. $^{64}CuCl_2$ was produced using a CS-15 biomedical cyclotron at Washington University School of Medicine by the ^{64}Ni(p,n)^{64}Cu nuclear reaction.

HPLC Methods

HPLC Method 1 used a LabAlliance semi-prep HPLC system (State College, PA) equipped with an UV/Vis detector (λ = 254 nm) and Zorbax C^{18} semi-prep column (9.4 mm × 250 mm, 100 Å pore size). The flow rate was 2.5 mL/min. The gradient mobile phase started with 90% solvent A (0.1% TFA in water) and 10% solvent B (0.1% TFA in acetonitrile) to 85% solvent A and 15% solvent B at 5 min to 65% solvent A and 35% solvent B at 30 min, followed by an isocratic mobile phase with 50% solvent A and 50% solvent B at 32 - 36 min. The radio-HPLC method (Method 2) used the LabAlliance semi-prep HPLC system equipped with a β-ram IN/US detector (Tampa, FL) and Zorbax C_{18} column (4.6 mm × 250 mm, 300 Å pore size; Agilent Technologies, Santa Clara, CA). The flow rate was 1 mL/min. The mobile phase was isocratic with 90% solvent A (25 mM ammonium acetate buffer, pH = 5.0) and 10% solvent B

(acetonitrile) at 0 - 2 min, followed by a gradient mobile phase going from 10% solvent B at 2 min to 15% solvent B at 5 min and to 20% solvent B at 20 min.

DOTA-PEG_4-E[PEG_4-c(RGDfK)]$_2$ (DOTA-3PEG_4-dimer)

DOTA-NHS (4.6 mg, 11 μmol) and PEG_4-E[PEG_4-c(RGDfK)]$_2$ (5 mg, 2.8 μmol) were dissolved in DMF (2 mL). After addition of triethylamine (10 mg, 10 μmol), the reaction mixture was stirred at room temperature overnight. The product was isolated from the mixture by HPLC purification (Method 1). The fraction at 19.5 min was collected. Lyophilization of the collected fractions afforded DOTA-3PEG_4-dimer as a white powder. The yield was 2.0 mg (~34%) with >95% HPLC purity. ESI-MS (positive mode): *m/z* = 1058.59 for $[M + H]^+$ (1058.99 calcd. for $[C_{77}H_{103}N_{23}O_{23}S]^+$).

DOTA-G_3-E[G_3-c(RGDfK)]$_2$ (DOTA-3G_3-dimer)

DOTA-3G_3-monomer was prepared using the same procedure using DOTA-NHS (4.4 mg, 10.6 μmol) and G_3-E[G_3-c(RGDfK)]$_2$ (3 mg, 3.53 μmol). Lyophilization of the combined collections at ~19.5 min (Method 1) afforded the expected product DOTA-3G_3-monomer. The yield was 1.6 mg (~40%) with HPLC purity >95%. ESI-MS: m/z=1154.17 for $[M+H]^+$ (1154.49 calcd. For $[C_{51}H_{72}N_{13}O_{16}S]^+$)

^{64}Cu-Labeling

To a 5 mL vial were added 50 μg of the DOTA-RGD conjugate (RGD = 3PEG_4-dimer or 3G_3-dimer) in 0.3 mL of 0.1 M NaOAc buffer (pH = 6.9) and 0.12 mL of $^{64}CuCl_2$ solution (~ 2.0 mCi) in 0.05 N HCl. The reaction mixture was heated at 100 °C for 30 min. After cooling to room temperature, a sample of resulting solution was analyzed by radio-HPLC (Method 2). The radiochemical purity (RCP) for ^{64}Cu(DOTA-3PEG_4-dimer) and ^{64}Cu(DOTA-3G_3-dimer) was >95% with the specific activity of 300 - 400 mCi/μmol.

Dose Preparation

For biodistribution studies, ^{64}Cu(DOTA-3PEG_4-dimer) and ^{64}Cu(DOTA-3G_3-dimer) were prepared, and then purified by HPLC (Method 2). Volatiles in the HPLC mobile phases were removed by rotary evaporation. The dose solution was prepared by dissolving the HPLC-purified radiotracer in saline to a concentration of 10 - 25 μCi/mL. In the blocking experiment, E[c(RGDfK)]$_2$ was dissolved in the solution containing the radiotracer to give a concentration of 1.75 mg/mL. For microPET imaging studies, ^{64}Cu(DOTA-3G_3-dimer) was prepared by using 12 μg of DOTA-3G_3-dimer to react with about 2 mCi of $^{64}CuCl_2$ in 0.3 mL of 0.1 M NaOAc buffer. After radiolabeling, ^{64}Cu(DOTA-3G_3-dimer) was purified with HPLC (Method 2). Volatiles in the HPLC mobile phases were removed by rotary evaporation. The residue was reconstituted in PBS to a concentration of ~1 mCi/mL. The resulting solution was filtered with a 0.20 μ Millex-LG filter before being injected into animals. Each tumor-bearing mouse was injected with 0.1 - 0.2 mL of the filtered dose solution.

Solution Stability

For solution stability studies, ^{64}Cu(DOTA-3PEG_4-dimer) and ^{64}Cu(DOTA-3G_3-dimer) were prepared and purified by HPLC (Method 2). Volatiles in the HPLC mobile phase were removed by rotary evaporation. The HPLC purified ^{64}Cu radiotracers were dissolved in 25 mM phosphate buffer (pH = 7.4) containing EDTA (1 mg/mL) to 1 mCi/mL. Samples of the resulting solution were analyzed by radio-HPLC (Method 2) at 0, 1, 2, 4 and 12 h post purification.

Determination of Log P Values

Log P values of were determined using the following procedure: the ^{64}Cu radiotracer was purified by HPLC. Volatiles were removed completely under vacuum. The residue was dissolved in a equal volume (3 mL:3 mL) mixture of n-octanol and 25 mM phosphate buffer (pH = 7.4). After stirring vigorously for ~20 min, the mixture was centrifuged at a speed of 8,000 rpm for 5 min. Samples (in triplets) from n-octanol and aqueous layers were counted in a Perkin Elmer Wizard - 1480 γ-counter (Shelton, CT). The log P value was measured three different times and reported as an average of three independent measurements plus the standard deviation.

In Vitro Whole-Cell Integrin $\alpha_v\beta_3$ Binding Assay

The *in vitro* integrin binding affinity and specificity of cyclic RGD peptides were assessed via a cellular displacement assay using ^{125}I-echistatin as the integrin-specific radioligand. Experiments were performed on U87MG glioma cell line by slight modification of a method previously described (50,52). Briefly, the U87MG glioma cells were grown in Gibco's Dulbecco's medium supplemented with 10% fetal bovine serum (FBS), 100 IU/ml penicillin and 100 μg/ml streptomycin (Invitrogen Co, Carlsbad, CA), at 37 °C in humidified atmosphere containing 5% CO_2. Filter multiscreen DV plates were seeded with 10^5 cells in binding buffer and incubated with ^{125}I-echistatin in the presence of increasing concentrations of cyclic RGD peptides. After removing the unbound ^{125}I-echistatin, hydrophilic PVDF filters were collected and the radioactivity was determined using a gamma counter (Packard, Meriden, CT). The IC_{50} values were calculated by fitting the data by nonlinear regression using GraphPad Prism™ (GraphPad Software, Inc., San Diego, CA), and reported as an average of these samples plus the standard deviation.

Animal Model and Biodistribution Protocol

Biodistribution studies were performed using the athymic nude mice bearing U87MG human glioma xenografts in compliance the NIH animal experiment guidelines (*Principles of Laboratory Animal Care*, NIH Publication No. 86-23, revised 1985. The protocol was approved by Purdue University Animal Care and Use Committee (PACUC). Female athymic nu/nu mice were purchased from Harlan (Charles River, MA) at 4 - 5 weeks of age. The mice were implanted with 5×10^6 the U87MG human glioma cells into the upper left flank. Two to three weeks after inoculation, the tumor size was 0.2 - 0.5 g, and animals were used for biodistribution and imaging studies. Sixteen tumor-bearing mice (20 - 25 g) were randomly divided into four groups. The ^{64}Cu radiotracer (~2.5 μCi in 0.1 mL saline) was administered into each animal via tail vein. Four animals were euthanized by sodium pentobarbital overdose (100 - 200 mg/kg), exsanguinations and opening of thoracic cavity at 5, 30, 60, and 120 min postinjection (p.i.). Blood samples were withdrawn from the heart through a syringe. Organs were excised, washed with saline, dried with absorbent tissue, weighed, and counted on a γ-counter (Perkin Elmer Wizard - 1480). Organs of interest included tumor, brain, spleen, lungs, liver, kidneys, muscle and intestine. The organ uptake was calculated as a percentage of the injected dose per gram of organ tissue (%ID/g). For the blocking experiment, each animal was administered with ~2.5 μCi of ^{64}Cu(DOTA-3PEG$_4$-dimer) along with ~350 μg of E[c(RGDfK)]$_2$ (~14 mg/kg). At 1 h p.i., four animals were sacrificed by sodium pentobarbital overdose (100 - 200 mg/kg) for organ biodistribution. The organ uptake (%ID/g) was compared to that obtained in the absence of excess E[c(RGDfK)]$_2$ at the same time point. The biodistribution data and target-to-background (T/B) ratios are reported as an average plus the standard variation based on results from four animals at each time point. Comparison between two different radiotracers was made using the two-way ANOVA test (GraphPad Prim 5.0, San Diego, CA). The level of significance was set at $p < 0.05$.

MicroPET Imaging

MicroPET imaging was performed using a microPET R4 rodent model scanner (Concorde Microsystems, Knoxville, TN). The U87MG glioma-bearing mice (n = 3) were injected with ~100 μCi of ^{64}Cu(DOTA-3G$_3$-dimer) via the tail vein, were then anesthetized with 2% isoflurane and placed near the center of the FOV where the highest resolution and sensitivity are obtained. The 5-min static PET images were obtained at 60 min p.i. For blocking experiment, a mouse bearing a U87MG tumor was injected with 100 μCi of ^{64}Cu (DOTA-3G$_3$-dimer) along with c(RGDyK) at the dose of 10 mg/kg. The 5-min static PET images were then acquired at 1 h p.i.

Metabolism

Normal athymic nude mice (n = 2) were used to evaluate the metabolic stability of ^{64}Cu (DOTA-3PEG$_4$-dimer) and ^{64}Cu(DOTA-3G$_3$-dimer). Each mouse was injected with the ^{64}Cu radiotracer at a dose of ~100 μCi in 0.2 mL saline via tail vein. The urine samples were collected at 30 and 120 min p.i. by manual void, and were mixed with equal volume of 20% acetonitrile aqueous solution. The mixture was centrifuged at 8,000 rpm. The supernatant was collected, counted on a Perkin Elmer Wizard - 1480 γ-counter, and filtered through a 0.20 μm Millex-LG filter unit. The filtrate was analyzed by radio-HPLC (Method 2). The feces samples were collected at 120 min p.i., and were suspended in the 20% acetonitrile aqueous solution. The mixture was vortexed for 5 - 10 min. After centrifuging at 8,000 rpm for 5 min, the supernatant was collected, counted on a Perkin Elmer Wizard - 1480 γ-counter, and passed through a 0.20 μm Millex-LG filter unit. The filtrate was then analyzed by radio-HPLC (Method 2). The percentage radioactivity recovery was >95% (by γ-counting) for both urine and feces samples.

RESULTS

Synthesis of DOTA-RGD Conjugates

DOTA-3PEG$_4$-dimer and DOTA-3G$_3$-dimer were prepared by direct conjugation of 3PEG$_4$-dimer and 3G$_3$-dimer, respectively, with excess DOTA-NHS in DMF in the presence of a base, such as triethylamine. DOTA-3PEG$_4$-dimer and DOTA-3G$_3$-dimer were purified by HPLC (Method 1) and characterized by ESI-MS. The mass spectral data were completely consistent with the proposed formula. Their HPLC purity was >95% before being used for the integrin $\alpha_v\beta_3$ binding assay and^{64}Cu-labeling.

Integrin $\alpha_v\beta_3$ Binding Affinity

The integrin $\alpha_v\beta_3$-positive U87MG human glioma cells were used for the integrin $\alpha_v\beta_3$-binding studies. We determined the integrin $\alpha_v\beta_3$ binding affinity of DOTA-3PEG$_4$-dimer and DOTA-3G$_3$-dimer by competitive displacement of ^{125}I-echistatin bound to U87MG glioma cells. For comparison purposes, we also evaluated DOTA-dimer and DOTA-tetramer using the same in vitro competition assay. The IC$_{50}$ values for DOTA-dimer, DOTA-3PEG$_4$-dimer, DOTA-3G$_3$-dimer and DOTA-tetramer were obtained from curve fitting from Figure 2, and were calculated to be 102 ± 5, 62 ± 6, 74 ± 3 and 10 ± 2 nM, respectively.

Radiochemistry

^{64}Cu(DOTA-3PEG$_4$-dimer) and ^{64}Cu(DOTA-3G$_3$-dimer) were prepared by reacting DOTA-3PEG$_4$-dimer and DOTA-3G$_3$-dimer, respectively, with ^{64}CuCl$_2$ in the 0.1 M NaOAc buffer (pH = 5.0). The ^{64}Cu-labeling could be accomplished by heating the reaction mixture at 100 °C for 20 - 30 min. Both ^{64}Cu(DOTA-3PEG$_4$-dimer) and ^{64}Cu(DOTA-3G$_3$-dimer) were analyzed using same radio-HPLC method (Method 2). Their HPLC retention times were 19.5 and 14.2 min, respectively. The RCP was >95% with the specific activity of 300 - 400 mCi/μmol for both ^{64}Cu(DOTA-3G$_3$-dimer) and ^{64}Cu(DOTA-3PEG$_4$-dimer). Their partition

coefficients (P values) were determined in an equal volume mixture of n-octanol and 25 mM phosphate buffer (pH = 7.4). The log P values were calculated to be -4.23 ± 0.21 and -4.84 ± 0.15, respectively, for ^{64}Cu(DOTA-3PEG$_4$-dimer) and ^{64}Cu(DOTA-3G$_3$-dimer). ^{64}Cu (DOTA-3PEG$_4$-dimer) and ^{64}Cu(DOTA-3G$_3$-dimer) were stable for >6 h after HPLC purification, and remained intact for >6 h without any decomposition in the presence of EDTA (1 mg/mL in 25 mM phosphate buffer, pH = 7.4).

Biodistribution Characteristics

Athymic nude mice bearing U87MG glioma xenografts were used to evaluate the biodistribution characteristics and excretion kinetics of ^{64}Cu(DOTA-3PEG$_4$-dimer) and ^{64}Cu (DOTA-3G$_3$-dimer). Figure 3 illustrates the %ID/g organ uptake for ^{64}Cu(DOTA-3G$_3$-dimer) and ^{64}Cu(DOTA-3PEG$_4$-dimer). In general, ^{64}Cu(DOTA-3G$_3$-dimer) had a rapid and very high tumor uptake at early time point (8.50 ± 1.44 %ID/g at 30 min p.i.). The tumor radioactivity washout of ^{64}Cu(DOTA-3G$_3$-dimer) was slow (7.55 ± 0.49 %ID/g, 7.43 ± 2.41 %ID/g and 6.79 ± 1.36 %ID/g at 60, 120 and 240 min p.i., respectively). Its blood clearance was very fast (2.17 ± 0.45 %ID/g at 30 min p.i. and 0.46 ± 0.15 %ID/g at 240 min p.i.) with the tumor/blood ratios increasing from 4.01 ± 1.13 at 30 min p.i. to 24.31 ± 2.20 %ID/g at 240 min p.i. The muscle uptake of ^{64}Cu(DOTA-3G$_3$-dimer) decreased steadily from 1.61 ± 0.66 %ID/g at 30 min p.i. to 0.86 ± 0.08 %ID/g at 240 min p.i. while the tumor/muscle ratios increased from 5.84 ± 2.49 at 30 min p.i. to 7.84 ± 1.15 at 240 min p.i. ^{64}Cu(DOTA-3G$_3$-dimer) also had a moderately high kidney uptake (8.83 ± 0.96 %ID/g) at 30 min p.i.; but its kidney clearance was very fast (3.23 ± 0.40 % ID/g at 240 min p.i.). The liver uptake of ^{64}Cu(DOTA-3G$_3$-dimer) was relatively low (2.60 ± 0.01 %ID/g) at 30 min p.i. To our surprise, its liver uptake increased over the 4 h study period (3.01 ± 0.51 %ID/g at 60 min and 3.62 ± 0.62 %ID/g at 240 min p.i.). As a result, its tumor/liver ratio slowly decreased from 3.27 ± 0.56 at 30 min to 1.93 ± 0.56 at 120 min p.i.

^{64}Cu(DOTA-3PEG$_4$-dimer) also had very high tumor uptake (8.23 ± 1.97 %ID/g, 6.49 ± 1.10 %ID/g, 7.55 ± 0.62 %ID/g and 6.43 ± 1.22 %ID/g at 30, 60, 120 and 240 min p.i., respectively) with fast blood clearance (0.87 ± 0.22 %ID/g at 30 min p.i. and 0.15 ± 0.07 %ID/g at 240 min p.i.). As a result, its tumor/blood ratios increased steadily from 9.8 ± 3.3 at 30 min p.i. to 46.3 ± 15.1 at 120 min p.i.). ^{64}Cu(DOTA-3PEG$_4$-dimer) had a relatively low initial kidney uptake (6.59 ± 0.93 %ID/g) at 30 min p.i. Its kidney uptake was 2.81 ± 0.36 % ID/g at 240 min p.i., and the tumor/kidney ratio was 2.28 ± 0.31. The liver uptake of ^{64}Cu(DOTA-3G$_3$-dimer) was also low (2.80 ± 0.35 %ID/g at 30 min p.i. and 1.87 ± 0.51 %ID/g at 240 min p.i.); but its tumor/liver ratio remained relatively unchanged over the 4 h study period (2.98 ± 0.86 at 30 min to 3.52 ± 0.61 at 240 min p.i.). The muscle uptake of ^{64}Cu(DOTA-3PEG$_4$-dimer) (1.28 ± 0.11 and 0.95 ± 0.34 %ID/g at 30 and 240 min p.i., respectively) was comparable to that of ^{64}Cu(DOTA-3G$_3$-dimer) (1.61 ± 0.66 and 0.86 ± 0.08 %ID/g at 30 and 240 min p.i., respectively). The tumor/muscle ratio of ^{64}Cu(DOTA-3PEG$_4$-dimer) increased steadily from 6.48 ± 1.54 at 30 min p.i. to 7.24 ± 2.08 at 240 min p.i.

Blocking Experiment

The integrin $\alpha_v\beta_3$ specificity was demonstrated by co-injection of excess E[c(RGDfK)]$_2$ as the blocking agent (~14 mg/kg or ~350 μg per mouse) with ^{64}Cu(DOTA-3G$_3$-dimer). Such a high dose was used to ensure that the integrin $\alpha_v\beta_3$ is almost completely blocked. Figure 4A shows organ uptake of ^{64}Cu(DOTA-3G$_3$-dimer) at 60 min p.i. in the absence/presence of E[c (RGDfK)]$_2$. Co-injection of excess E[c(RGDfK)]$_2$ resulted in almost complete blockage of tumor uptake for ^{64}Cu(DOTA-3G$_3$-dimer) (0.43 ± 0.07 %ID/g with E[c(RGDfK)]$_2$ vs. 7.43 ± 2.41 %ID/g without E[c(RGDfK)]$_2$). There was also a significant reduction in organ uptake of ^{64}Cu(DOTA-3G$_3$-dimer) in the eyes, heart, intestine, kidneys, lungs, liver and spleen (Figure 4A).

MicroPET Imaging

Figure 4B illustrates the representative microPET images of the glioma-bearing mice at 1 h after administration of ~100 μCi of ^{64}Cu(DOTA-3G$_3$-dimer) in the absence or presence of excess E[c(RGDfK)]$_2$. We found that the tumor was clearly visualized with excellent contrast, suggesting that ^{64}Cu(DOTA-3G$_3$-dimer) is useful for imaging integrin $\alpha_v\beta_3$-positive tumors. In the presence of excess E[c(RGDfK)]$_2$, the tumor uptake of ^{64}Cu(DOTA-3G$_3$-dimer) was almost completely blocked. The uptake of ^{64}Cu(DOTA-3G$_3$-dimer) was also blocked in many normal organs, in accordance with the biodistribution results shown in Figure 4A.

Tumor Size vs. Tumor Uptake

During the biodistribution studies, we noticed that smaller tumors (< 0.5 g) often have higher radiotracer uptake than large tumors. To further clarify the relationship between the tumor uptake and tumor size, we added five extra glioma-bearing mice into the 120 min group for ^{64}Cu(DOTA-3PEG$_4$-dimer). The 120-min time point was chosen to avoid potential interference from the blood radioactivity and non-specific radioactivity accumulation in the tumors. As illustrated in Figure 5A, there was a linear relationship between the %ID tumor uptake of ^{64}Cu(DOTA-3PEG$_4$-dimer) and the tumor size (0.03 - 0.8 g; n = 7; tumor number = 14) with R^2 = 0.9375. The radiotracer %ID tumor uptake increases when tumor size increases. If the tumor uptake is expressed as %/ID/g (Figure 5B), ^{64}Cu(DOTA-3PEG$_4$-dimer) had the %ID/g tumor uptake (6.5 - 10.0 %ID/g) with the tumor size in the range of 0.09 g - 0.25 g. When the tumor size is >0.30 g, the tumor uptake of ^{64}Cu(DOTA-3PEG$_4$-dimer) was in the range of 6.0 - 7.0 %ID/g. When the tumor size was <0.05 g, its tumor uptake was <5.0 %ID/g.

Metabolic Properties

Figure 6 shows HPLC chromatograms of ^{64}Cu(DOTA-3PEG$_4$-dimer) (left) and ^{64}Cu (DOTA-3G$_3$-dimer) (right) in saline before injection, in urine at 30 min p.i. and 120 min p.i., and in feces at 120 min p.i. There were no metabolites detected in either urine and or feces samples from the mouse administered with ^{64}Cu(DOTA-3PEG$_4$-dimer). No metabolites were detected in the urine samples of the mouse administered with ^{64}Cu(DOTA-3G$_3$-dimer); but there was no intact ^{64}Cu(DOTA-3G$_3$-dimer) in the feces sample.

DISCUSSION

Previously, we reported the evaluation of ^{64}Cu-DOTA-dimer and ^{64}Cu-DOTA-tetramer as PET radiotracers for imaging integrin $\alpha_v\beta_3$ expression in athymic nude mice bearing MDA-MB-435 breast cancer and U87MG glioma xenografts (50,52). The biodistribution studies clearly demonstrate that ^{64}Cu-DOTA-dimer and ^{64}Cu-DOTA-tetramer have better tumor uptake with longer tumor retention time than their monomeric counterparts. In this study, we prepared two new RGD dimer DOTA conjugates (DOTA-3PEG$_4$-dimer and DOTA-3G$_3$-dimer) and their ^{64}Cu complexes, ^{64}Cu(DOTA-3PEG$_4$-dimer) and ^{64}Cu(DOTA-3G$_3$-dimer). The in vitro competition assay shows that the integrin $\alpha_v\beta_3$ binding affinities of cyclic RGD peptide conjugates follow the order of DOTA-tetramer > DOTA-3G$_3$-dimer ~ DOTA-3PEG$_4$-dimer > DOTA-dimer. DOTA-3G$_3$-dimer (IC_{50} = 62 ± 6 nM) and DOTA-3PEG$_4$-dimer (IC_{50} = 74 ± 3 nM) share very similar integrin $\alpha_v\beta_3$ binding affinity with HYNIC-3G3-dimer (IC_{50} = 61 ± 2 nM) and HYNIC-3PEG$_4$-dimer (IC_{50} = 51 ± 7 nM) (72, 73). Apparently, replacing HYNIC with DOTA does not have significant impact on their integrin $\alpha_v\beta_3$ binding affinity and the radiotracer tumor uptake. This may explain why ^{64}Cu (DOTA-3PEG$_4$-dimer) and ^{64}Cu(DOTA-3G$_3$-dimer) have the tumor uptake very similar to that of ^{99m}Tc-3PEG$_4$-dimer and ^{99m}Tc-3G$_3$-dimer (72,73).

There are two factors contributing to their high integrin $\alpha_v\beta_3$ binding affinity (Figure 1). The key for bivalency is that the distance between two RGD motifs in multimeric cyclic RGD peptides must be long enough to achieve simultaneous integrin $\alpha_v\beta_3$ binding. The distance between two cyclic RGD motifs is 6 bonds in E[c(RGDfK)]$_2$, 26 bonds in 3G$_3$-dimer and 38 bonds in 3PEG$_4$-dimer (excluding side arms of K-residues). The higher integrin $\alpha_v\beta_3$ binding affinity of DOTA-3G$_3$-dimer (IC_{50} = 62 ± 6 nM) and DOTA-3PEG$_3$-dimer (IC_{50} = 74 ± 3 nM) than that of DOTA-dimer (IC_{50} = 102 ± 5 nM) strongly suggests that 2G$_3$-dimer and 3PEG$_3$-dimer are bivalent in binding to integrin $\alpha_v\beta_3$ (Figure 1A), and that the distance between the two cyclic RGD motifs in E[c(RGDfK)]$_2$ is probably too short for simultaneous integrin $\alpha_v\beta_3$ binding. This conclusion is well supported by the significantly higher tumor uptake of ^{64}Cu(DOTA-3PEG$_4$-dimer) (8.50 ± 1.44 %ID/g and 6.79 ± 1.36 %ID/g at 30 and 240 min p.i., respectively) and ^{64}Cu(DOTA-3G$_3$-dimer) (8.23 ± 1.97 %ID/g and 6.43 ± 1.22 %ID/g at 30 and 240 min p.i., respectively) as compared to that of ^{64}Cu(DOTA-dimer) (3.23 ± 0.57 %ID/g at 30 min and 3.83 ± 0.22 %ID/g at 240 min p.i.) in the same tumor-bearing animal model (50). If DOTA-dimer were able to bind to integrin $\alpha_v\beta_3$ in the bivalent fashion as DOTA-2G$_3$-dimer and DOTA-3PEG$_3$-dimer, they would have shared a similar integrin $\alpha_v\beta_3$ binding affinity, and ^{64}Cu(DOTA-dimer) would have had the similar tumor uptake as ^{64}Cu(DOTA-3PEG-dimer) and ^{64}Cu(DOTA-3G$_3$-dimer). Even though DOTA-dimer is not bivalent, the binding of one cyclic RGD motif in E[c(RGDfK)]$_2$ may significantly increase "local RGD concentration" in the vicinity of neighboring integrin $\alpha_v\beta_3$ sites (Figure 1B). This may explain why ^{64}Cu(DOTA-dimer) has better tumor uptake than its monomeric counter part (50).

The longest distance between the two adjacent cyclic RGD motifs in E[E[c(RGDfK)]2]$_2$ is 16 bonds (excluding side arms of K-residues). The integrin $\alpha_v\beta_3$ binding affinity of DOTA-tetramer (IC_{50} = 10 ± 2 nM) is higher than that of DOTA-3G$_3$-dimer (IC_{50} = 62 ± 6 nM) and DOTA-3PEG$_3$-dimer (IC_{50} = 74 ± 3 nM), suggesting that DOTA-tetramer is also bivalent in binding to integrin $\alpha_v\beta_3$. The higher integrin $\alpha_v\beta_3$ binding affinity of DOTA-tetramer as compared to DOTA-3G$_3$-dimer and DOTA-3PEG$_3$-dimer is probably caused by the presence of two extra RGD motifs. This conclusion seems to be consistent with the fact that ^{64}Cu(DOTA-tetramer) has higher initial tumor uptake (9.93 ± 1.05 %ID/g at 30 min p.i.) as compared to that of ^{64}Cu(DOTA-3PEG$_4$-dimer) (8.50 ± 1.44 %ID/g at 30 min p.i.) and ^{64}Cu(DOTA-3G$_3$-dimer) (8.23 ± 1.97 %ID/g at 30 min p.i.) in the same tumor-bearing animal model.

However, ^{64}Cu(DOTA-3PEG$_4$-dimer) and ^{64}Cu(DOTA-3G$_3$-dimer) have significant advantages over ^{64}Cu(DOTA-tetramer) with respect to their uptake in non-cancerous organs. For example, the liver uptake of ^{64}Cu(DOTA-3PEG$_4$-dimer) (2.25 ± 0.26 %ID/g at 60 min p.i. and 1.87 ± 0.51 %ID/g at 240 min p.i.) was significantly lower ($p < 0.01$) than that of ^{64}Cu(DOTA-tetramer) (4.38 ± 0.39 %ID/g at 60 min p.i. and 3.57 ± 0.45 %ID/g at 240 min p.i.) (52). As a result, the tumor/liver ratios of ^{64}Cu(DOTA-3PEG$_4$-dimer) (2.93 ± 0.66 at 60 min and 3.52 ± 0.61 at 240 min p.i.) were significantly better ($p < 0.01$) than that of ^{64}Cu(DOTA-tetramer) (1.98 ± 0.15 at 60 min p.i. and 2.35 ± 0.33 at 240 min p.i.). ^{64}Cu(DOTA-3PEG$_4$-dimer) has significantly ($p < 0.01$) lower kidney uptake (6.59 ± 0.93 %ID/g at 30 min p.i. and 2.81 ± 0.36 %ID/g at 240 min p.i.) than ^{64}Cu(DOTA-tetramer) (9.02 ± 0.56 %ID/g at 30 min p.i. and 4.17 ± 0.35 %ID/g at 240 min p.i.). The higher kidney uptake of ^{64}Cu(DOTA-tetramer) is probably caused by the presence of four R-residues, which are positively charged under physiological conditions, in E{E[c(RGDfK)]$_2$}$_2$ as compare to only two R-residues in both ^{64}Cu(DOTA-3PEG$_4$-dimer) and ^{64}Cu(DOTA-3G$_3$-dimer). On the basis of both tumor uptake and T/B ratios of ^{64}Cu radiotracers, we believe that 3PEG$_4$-dimer and 3G$_3$-dimer are better targeting biomolecules than E{E[c(RGDfK)]$_2$}$_2$. In addition, synthesis of E{E[c(RGDfK)]$_2$}$_2$ is much more challenging than that of either 3PEG$_4$-dimer or 3G$_3$-dimer. The cost for successful isolation of pure multimeric cyclic RGDfK peptides increases dramatically

as the peptide multiplicity increases. Therefore, 3PEG$_4$-dimer and 3G$_3$-dimer are better suited for future development of the integrin $\alpha_v\beta_3$-targeted radiotracers for imaging purposes.

Since the tumor uptake of ^{64}Cu(DOTA-3PEG$_4$-dimer) is almost completely blocked by co-injection of E[c(RGDfK)]$_2$, we believe that its tumor localization is indeed integrin $\alpha_v\beta_3$-mediated. Similar results were obtained for ^{64}Cu(DOTA-dimer) in athymic nude mice bearing MDA-MB-435 human breast cancer xenografts (50), and ^{64}Cu(DOTA-tetramer) in athymic nude mice bearing U87MG human glioma xenografts (52). The uptake blockage in the eyes, heart, intestine, lungs, liver and spleen suggests that major parts of the uptake of ^{64}Cu (DOTA-3PEG$_4$-dimer) in these organs is also integrin $\alpha_v\beta_3$-mediated. This conclusion is supported by the immunohistopathological studies (53,54), which showed a strong positive staining of endothelial cells of the small glomeruli vessels in the kidneys and weak staining in the branches of the hepatic portal vein.

The ability to non-invasively quantify integrin $\alpha_v\beta_3$ level in vivo will provide new opportunities to more appropriately select patients for anti-angiogenic treatment and more effectively monitor the therapeutic efficacy in integrin $\alpha_v\beta_3$-positive cancer patients (34). The %ID tumor uptake reflects the total integrin $\alpha_v\beta_3$ expression level while the %ID/g tumor uptake reflects the integrin $\alpha_v\beta_3$ density. When the tumor is very small (<0.01 g or 100 m^3), there is little angiogenesis with very low blood flow. As a result, ^{64}Cu(DOTA-3PEG$_4$-dimer) has low %ID and %ID/g tumor uptake (Figure 5: A and B). When tumors are in the range of 0.1 - 0.35 g (100 - 350 m^3), the microvessel and integrin $\alpha_v\beta_3$ density is high. The radiotracer %ID/g tumor uptake is high (Figure 5B) even though the %ID tumor uptake is relatively low (Figure 5A). As tumors grow, the total integrin $\alpha_v\beta_3$ level on tumor cells becomes larger, the microvessel density decreases due to maturity of blood vessels, and the integrin $\alpha_v\beta_3$ density also decreases due to larger interstitial space/pressure and higher collagen concentrations (78). Parts of the tumor may become necrotic, which also leads to lower integrin $\alpha_v\beta_3$ density in larger tumors. As a result, the %ID/g tumor uptake of ^{64}Cu(DOTA-3PEG$_4$-dimer) in larger tumors is lower than that of smaller ones (Figure 5B) even though its total %ID tumor uptake is higher (Figure 5A). The linear relationship between tumor size and %ID tumor uptake suggests that ^{64}Cu (DOTA-3PEG$_4$-dimer) might be useful for non-invasive monitoring of integrin $\alpha_v\beta_3$ expression in cancer patients. This assumption is supported by recent results obtained for the radiolabeled (^{18}F and ^{64}Cu) multimeric cyclic RGDyK peptides, which clearly showed that the %ID/g radiotracer tumor uptake was well correlated with the integrin $\alpha_v\beta_3$ density on the xenografted tumors of different origin (52,53).

Metabolic degradation has been observed for ^{64}Cu(DOTA-dimer) and ^{64}Cu(DOTA-tetramer) in kidneys and urine samples (50,52). In contrast, ^{64}Cu(DOTA-3PEG$_4$-dimer) has high metabolic stability during its excretion from the renal and hepatobiliary routes (Figure 6). Similar metabolic stability is also observed for ^{64}Cu(DOTA-3G$_3$-dimer) during its renal excretion; but it is completely metabolized during excretion from the hepatobiliary route. The PEG$_4$ and G$_3$ linkers have significant impact on metabolic stability of ^{64}Cu-labeled RGD dimers probably due to in vivo stability PEG$_4$ and G$_3$ linkers. It is important to note that the radioactivity detected in urine and feces samples represents only the portion of ^{64}Cu radiotracers excreted from renal and hepatobiliary routes. The remaining radioactivity is still “trapped” in normal tissues. Since the normal organ uptake of ^{64}Cu(DOTA-3PEG$_4$-dimer) can be blocked by the presence of excess E[c(RGDfK)]$_2$, it is reasonable to believe that the radioactivity accumulation inside normal organs is partially integrin $\alpha_v\beta_3$-mediated.

CONCLUSION

In this study, we prepared two novel cyclic RGD dimer conjugates: DOTA-3PEG$_4$-dimer and DOTA-3G$_3$-dimer. The integrin $\alpha_v\beta_3$ binding affinities follow the order of DOTA-tetramer >

DOTA-$3G_3$-dimer ~ DOTA-$3PEG_4$-dimer > DOTA-dimer. Both DOTA-$3G_3$-dimer and DOTA-$3PEG_4$-dimer are bivalent in binding to integrin $\alpha_v\beta_3$, as evidenced by their higher integrin $\alpha_v\beta_3$ binding affinity as compared to that of DOTA-dimer and the higher tumor uptake of ^{64}Cu(DOTA-$3PEG_4$-dimer) and ^{64}Cu(DOTA-$3G_3$-dimer) than that of ^{64}Cu(DOTA-dimer). The PEG_4 and G_3 linkers are also useful for improving the radiotracer clearance from normal organs, such as kidneys, liver and lungs. The ex-vivo biodistribution studies show that there is a linear relationship between the %ID tumor uptake and tumor size, suggesting that ^{64}Cu (DOTA-3PEG-dimer) and ^{64}Cu(DOTA-$3G_3$-dimer) might be useful for noninvasive monitoring of tumor growth or shrinkage during anti-angiogenic therapy. MicroPET imaging data clearly demonstrate utility of ^{64}Cu(DOTA-$3G_3$-dimer) as a new PET radiotracer for imaging integrin $\alpha_v\beta_3$-positive tumors.

ACKNOWLEDGMENT

Authors would like to thank Dr. Sulma I. Mohammed, the Director of Purdue Cancer Center Drug Discovery Shared Resource, for her assistance with tumor-bearing animal models. This work is supported, in part, by research grants: R01 CA115883 A2 (S.L.) from National Cancer Institute (NCI), R21 HL083961-01 from National Heart, Lung, and Blood Institute (NHLBI), and DE-FG02-08ER64684 from the Department of Energy. The research performed at Stanford University is supported, in part, by NCI R01 CA119053, R21 CA121842, P50 CA114747, U54 CA119367 and R24 CA93862.

REFERENCES

(1). Folkman J. Angiogenesis in cancer, vascular, rheumatoid and other disease. Nat. Med 1995;1:27–31. [PubMed: 7584949]

(2). Folkman J. Role of angiogenesis in tumor growth and metastasis. Semin. Oncol 2002;29:15–18. [PubMed: 12516034]

(3). Mousa SA. Mechanisms of angiogenesis in vascular disorders: potential therapeutic targets. Drugs of the Future 1998;23:51–60.

(4). Mousa SA. Integrins as novel drug discovery targets: potential therapeutic and diagnostic implications. Emerging Therapeutic Targets 2000;4:143–153.

(5). Carmeliet P. Mechanism of angiogenesis and atheriogenesis. Nat. Med 2000;6:389–395. [PubMed: 10742145]

(6). Devita V, Hellman S, Bögler O, Mikkelsen T. Angiogenesis in Glioma: molecular mechanisms and roadblocks to translation. Cancer J 2003;9:205–213. [PubMed: 12952305]

(7). Hwang R, Varner JV. The role of integrins in tumor angiogenesis. Hematol. Oncol. Clin. North. Am 2004;18:991–1006. [PubMed: 15474331]

(8). Jin H, Varner J. Integrins: roles in cancer development and as treatment targets. Br. J. Cancer 2004;90:561–565. [PubMed: 14760364]

(9). Kumar CC. Integrin $\alpha_v\beta_3$ as a therapeutic target for blocking tumor-induced angiogenesis. Curr. Drug Targets 2003;4:123–131. [PubMed: 12558065]

(10). Brooks PC, Clark RAF, Cheresh DA. Requirement of vascular integrin $\alpha_v\beta_3$ for angiogenesis. Science 1994;264:569–571. [PubMed: 7512751]

(11). Friedlander M, Brooks PC, Shatter RW, Kincaid CM, Varner JA, Cheresh DA. Definition of two angiogenic pathways by distinct α_v integrin. Science 1995;270:1500–1502. [PubMed: 7491498]

(12). Horton MA. The $\alpha_v\beta_3$ integrin “vitronectin receptor”. Int. J. Biochem. Cell Biol 1997;29:721–725. [PubMed: 9251239]

(13). Bello L, Francolini M, Marthyn P, Zhang JP, Carroll RS, Nikas DC, Strasser JF, Villani R, Cheresh DA, Black PM. Alpha(v)beta3 and alpha(v)beta5 integrin expression in glioma periphery. Neurosurgery 2001;49:380–389. [PubMed: 11504114]

(14). Meitar D, Crawford SE, Rademaker AW, Cohn SL. Tumor angiogenesis correlates with metastatic disease, N-*myc*-amplification, and poor outcome in human neuroblastoma. J. Clinical. Oncol 1996;14:405–414. [PubMed: 8636750]

(15). Gasparini G, Brooks PC, Biganzoli E, Vermeulen PB, Bonoldi E, Dirix LY, Ranieri G, Miceli R, Cheresh DA. Vascular integrin $\alpha_v\beta_3$: a new prognostic indicator in breast cancer. Clin. Cancer Res 1998;4:2625–2634. [PubMed: 9829725]

(16). Albelda SM, Mette SA, Elder DE, Stewart RM, Damjanovich L, Herlyn M, Buck CA. Integrin distribution in maliganant melanoma: association of the beta3 subunit with tumor progression. Cancer Res 1990;50:6757–6764. [PubMed: 2208139]

(17). Falcioni R, Cimino L, Gentileschi MP, D'Agnano I, Zupi G, Kennel SJ, Sacchi A. Expression of beta 1, beta 3, beta 4, and beta 5 integrins by human lung carcinoma cells of different histotypes. Exp. Cell Res 1994;210:113–122. [PubMed: 7505746]

(18). Sengupta S, Chattopadhyay N, Mitra A, Ray S, Dasgupta S, Chatterjee A. Role of $\alpha_v\beta_3$ integrin receptors in breast tumor. J. Exp. Clin. Cancer Res 2001;20:585–590. [PubMed: 11876555]

(19). Felding-Habermann B, Mueller BM, Romerdahl CA, Cheresh DA. Involvement of integrin alpha V gene expression in human melanoma tumorigenicity. J. Clin. Invest 1992;89:2018–2022. [PubMed: 1376331]

(20). Zitzmann S, Ehemann V, Schwab M. Arginine-Glycine-Aspartic acid (RGD)-peptide binds to both tumor and tumor endothelial cells in vivo. Cancer Res 2002;62:5139–5143. [PubMed: 12234975]

(21). Weber WA, Haubner R, Vabuliene E, Kuhnast B, Webster HJ, Schwaiger M. Tumor angiogenesis targeting using imaging agents. Q. J. Nucl. Med 2001;45:179–182. [PubMed: 11476168]

(22). Costouros NG, Diehn FE, Libutti SK. Molecular imaging of tumor angiogenesis. J. Cell. Biochem. Suppl 2002;39:72–78. [PubMed: 12552605]

(23). Liu S, Edwards DS. Fundamentals of receptor-based diagnostic metalloradiopharmaceuticals. Topics in Current Chem 2002;222:259–278.

(24). Van de Wiele C, Oltenfreiter R, De Winter O, Signore A, Slegers G, Dieckx RA. Tumor angiogenesis pathways: related clinical issues and implications for nuclear medicine imaging. Eur. J. Nucl. Med 2002;29:699–709.

(25). Liu S, Robinson SP, Edwards DS. Integrin $\alpha_v\beta_3$ directed radiopharmaceuticals for tumor imaging. Drugs of the Future 2003;28:551–564.

(26). McDonald DM, Choyke P. Imaging of Angiogenesis: from microscope to clinic. Nature Med 2003;9:713–725. [PubMed: 12778170]

(27). Haubner R, Wester HR. Radiolabeled tracers for imaging of tumor angiogenesis and evaluation of anti-angiogenic therapies. Curr. Pharm. Des 2004;10:1439–1455. [PubMed: 15134568]

(28). Liu S, Robinson SP, Edwards DS. Radiolabeled integrin $\alpha_v\beta_3$ antagonists as radiopharmaceuticals for tumor radiotherapy. Topics in Current Chem 2005;252:193–216.

(29). Chen X. Multimodality imaging of tumor integrin $\alpha_v\beta_3$ expression. Mini-Rev. Med. Chem 2006;6:227–234. [PubMed: 16472190]

(30). D'Andrea LD, Del Gatto A, Pedone C, Benedetti E. Peptide-based molecules in angiogenesis. Chem. Biol. Drug Des 2006;67:115–126. [PubMed: 16492159]

(31). Meyer A, Auremheimer J, Modlinger A, Kessler H. Targeting RGD recognizing integrins: drug development, biomaterial research, tumor imaging and targeting. Curr. Pharm. Design 2006;12:2723–2747.

(32). Liu S. Radiolabeled multimeric cyclic RGD peptides as integrin $\alpha_v\beta_3$-targeted radiotracers for tumor imaging. Mol. Pharm 2006;3:472–487. [PubMed: 17009846]

(33). Cai W, Chen X. Multimodality Molecular imaging of tumor angiogenesis. J. Nucl. Med 2008;49:113S–128S. [PubMed: 18523069]

(34). Cai W, Rao J, Gambhir SS, Chen X. How molecular imaging is speeding up antiangiogenic drug development. Mol. Cancer Ther 2006;5:2624–2633. [PubMed: 17121909]

(35). Haubner R, Wester HJ, Senekowitsch-Schmidtke R, Diefenbach B, Kessler H, Stöcklin G, Schwaiger M. RGD-peptides for tumor targeting: biological evaluation of radioiodinated analogs and introduction of a novel glycosylated peptide with improved biokinetics. J. Labelled Compounds & Radiopharmaceuticals 1997;40:383–385.

(36). Haubner R, Bruchertseifer F, Bock M, Schwaiger M, Wester HJ. Synthesis and biological evaluation of ^{99m}Tc-labeled cyclic RGD peptide for imaging integrin $\alpha_v\beta_3$ expression. Nuklearmedizin 2004;43:26–32. [PubMed: 14978538]2004

(37). Haubner R, Wester HJ, Reuning U, Senekowitsch-Schmidtke R, Diefenbach B, Kessler H, Stöcklin G, Schwaiger M. Radiolabeled $\alpha_v\beta_3$ integrin antagonists: a new class of tracers for tumor imaging. J. Nucl. Med 1999;40:1061–1071. [PubMed: 10452325]

(38). Sivolapenko GB, Skarlos D, Pectasides D, Stathopoulou E, Milonakis A, Sirmalis G, Stuttle A, Courtenay-Luck NS, Konstantinides K, Epenetos AA. Imaging of metastatic melanoma utilizing a technetium-99m labeled RGD-containing synthetic peptide. Eur. J. Nucl. Med 1998;25:1383–1389. [PubMed: 9818277]

(39). Haubner R, Wester HJ, Burkhart F, Senekowitsch-Schmidtke R, Weber W, Goodman SL, Kessler H, Schwaiger M. Glycosylated RGD-containing peptides: tracer for tumor targeting and angiogenesis imaging with improved biokinetics. J. Nucl. Med 2001;42:326–336. [PubMed: 11216533]

(40). Haubner R, Wester HJ, Weber WA, Mang C, Ziegler SI, Goodman SL, Senekowitsch-Schmidtke R, Kessler H, Schwaiger M. Noninvasive imaging of $\alpha_v\beta_3$ integrin expression using ^{18}F-labeled RGD-containing glycopeptide and positron emission tomography. Cancer Res 2001;61:1781–1785. [PubMed: 11280722]

(41). Thumshirn G, Hersel U, Goodman SL, Kessler H. Multimeric cyclic RGD peptides as potential tools for tumor targeting: solid-phase peptide synthesis and chemoselective oxime ligation. Chem. Eur. J 2003;9:2717–2725.

(42). Poethko T, Schottelius M, Thumshirn G, Herz M, Haubner R, Henriksen G, Kessler H, Schwaiger M, Wester HJ. Chemoselective pre-conjugate radiohalogenation of unprotected mono-and multimeric peptides via oxime formation. Radiochim. Acta 2004;92:317–327.

(43). Poethko T, Schottelius M, Thumshirn G, Hersel U, Herz M, Henriksen G, Kessler H, Schwaiger M, Wester HJ. Two-step methodology for high yield routine radiohalogenation of peptides: ^{18}F-labeled RGD and octreotide analogs. J. Nucl. Med 2004;45:892–902. [PubMed: 15136641]

(44). Alves S, Correia JDG, Gano L, Rold TL, Prasanphanich A, Haubner R, Rupprich M, Alberto R, Decristoforo C, Snatos I, Smith CJ. In vitro and in vivo evaluation of a novel ^{99m}Tc(CO)$_3$-pyrazolyl conjugate of *cyclo*-(Arg-Gly-Asp-D-Tyr-Lys). Bioconj. Chem 2007;18:530–537.

(45). Su ZF, Liu G, Gupta S, Zhu Z, Rusckowski M, Hnatowich DJ. In vitro and in vivo evaluation of a technetium-99m-labeled cyclic RGD peptide as specific marker of $\alpha_v\beta_3$ integrin for tumor imaging. Bioconj. Chem 2002;13:561–570.

(46). Decristoforo C, Faintuch-Linkowski B, Rey A, vo Guggenberg E, Rupprich M, Hernandez-Gonzales I, Rodrigo T, Haubner R. [^{99m}Tc]HYNIC-RGD for imaging integrin $\alpha_v\beta_3$ expression. Nucl. Med. Biol 2006;33:945–952. [PubMed: 17127166]

(47). Chen X, Park R, Tohme M, Shahinian AH, Bading JR, Conti PS. MicroPET and autoradiographic imaging of breast cancer α_v-integrin expression using ^{18}F- and ^{64}Cu-labeled RGD peptide. Bioconj. Chem 2004;15:41–49.

(48). Chen X, Park R, Shahinian AH, Tohme M, Khankaldyyan V, Bozorgzadeh MH, Bading JR, Moats R, Laug WE, Conti PS. ^{18}F-labeled RGD peptide: initial evaluation for imaging brain tumor Angiogenesis. Nucl. Med. Biol 2004;31:179–189. [PubMed: 15013483]

(49). Chen X, Park R, Shahinian AH, Bading JR, Conti PS. Pharmacokinetics and tumor retention of ^{125}I-labeled RGD peptide are improved by PEGylation. Nucl. Med. Biol 2004;31:11–19. [PubMed: 14741566]

(50). Chen X, Liu S, Hou Y, Tohme M, Park R, Bading JR, Conti PS. MicroPET imaging of breast cancer α_v-integrin expression with ^{64}Cu-labeled dimeric RGD peptides. Mol. Imag. Biol 2004;6:350–359.

(51). Chen X, Tohme M, Park R, Hou Y, Bading JR, Conti PS. MicroPET imaging of breast cancer $\alpha_v\beta_3$-integrin expression with ^{18}F-labeled dimeric RGD peptide. Mol.Imaging 2004;3:96–104. [PubMed: 15296674]

(52). Wu Y, Zhang X, Xiong Z, Cheng Z, Fisher DR, Liu S, Gambhir SS, Chen X. MicroPET imaging of glioma integrin $\alpha_v\beta_3$ expression using ^{64}Cu-labeled tetrameric RGD peptide. J. Nucl. Med 2005;46:1707–1718. [PubMed: 16204722]

(53). Zhang X, Xiong Z, Wu Y, Cai W, Tseng JR, Gambhir SS, Chen X. Quantitative PET imaging of tumor integrin $\alpha_v\beta_3$ expression with ^{18}F-FPRGD2. J. Nucl. Med 2006;47:113–121. [PubMed: 16391195]

(54). Wu Z, Li Z, Chen K, Cai W, He L, Chin FT, Li F, Chen X. Micro-PET of tumor integrin $\alpha_v\beta_3$ expression using ^{18}F-labeled PEGylated tetrameric RGD peptide (FFPRGD4). J. Nucl. Med 2007;48:1536–1544. [PubMed: 17704249]

(55). Zhang X, Chen X. Preparation and characterization of ^{99m}Tc(CO)$_3$-BPy-RGD complex as $\alpha_v\beta_3$ integrin receptor-targeted imaging agent. Appl. Radiat. Isotopes 2007;65:70–78.

(56). Liu S, Edwards DS, Ziegler MC, Harris AR, Hemingway SJ, Barrett JA. ^{99m}Tc-Labeling of a hydrazinonictotinamide-conjugated vitronectin receptor antagonist for imaging tumors. Bioconj. Chem 2001;12:624–629.

(57). Liu S, Hsieh WY, Kim YS, Mohammed SI. Effect of coligands on biodistribution characteristics of ternary ligand ^{99m}Tc complexes of a HYNIC-conjugated cyclic RGDfK dimer. Bioconj. Chem 2005;16:1580–1588.

(58). Jia B, Shi J, Yang Z, Xu B, Liu Z, Zhao H, Liu S, Wang F. ^{99m}Tc-labeled cyclic RGDfK dimer: initial evaluation for SPECT imaging of glioma integrin $\alpha_v\beta_3$ expression. Bioconj. Chem 2006;17:1069–1076.

(59). Liu S, He Z, Hsieh WY, Kim YS, Jiang Y. Impact of PKM linkers on biodistribution characteristics of the ^{99m}Tc-labeled cyclic RGDfK dimer. Bioconj. Chem 2006;17:1499–1507.

(60). Liu S, Hsieh WY, Jiang Y, Kim YS, Sreerama SG, Chen X, Jia B, Wang F. Evaluation of a ^{99m}Tc-labeled cyclic RGD tetramer for non-invasive imaging integrin $\alpha_v\beta_3$-positive breast cancer. Bioconj. Chem 2007;18:438–446.

(61). Liu S, Kim YS, Hsieh WY, Sreerama SG. Coligand effects on solution stability, biodistribution and metabolism of ^{99m}Tc-labeled cyclic RGDfK tetramer. Nucl. Med. Biol 2008;35:111–121. [PubMed: 18158950]

(62). Jia B, Liu Z, Liu ZF, Yu ZL, Yang Z, Zhao HY, He ZJ, Liu S, Wang F. Linker effects on biological properties of ^{111}In-labeled DTPA conjugates of a cyclic RGDfK dimer. Bioconj. Chem 2008;19:201–210.

(63). Wang JJ, Kim YS, Liu S. ^{99m}Tc-labeling of HYNIC-conjugated cyclic RGDfK dimer and tetramer using EDDA as coligand. Bioconj. Chem 2008;19:634–642.

(64). Janssen ML, Oyen WJG, Dijkgraaf I, Massuger LF, Frielink C, Edwards DS, Rajopadhye M, Boonstra H, Corstens FH, Boerman OC. Tumor targeting with radiolabeled $\alpha_v\beta_3$ integrin binding peptides in a nude mouse model. Cancer Res 2002;62:6146–6151. [PubMed: 12414640]

(65). Janssen M, Oyen WJG, Massuger LFAG, Frielink C, Dijkgraaf I, Edwards DS, Rajopadhye M, Corsten FHM, Boerman OC. Comparison of a monomeric and dimeric radiolabeled RGD-peptide for tumor targeting. Cancer Biother. Radiopharm 2002;17:641–646. [PubMed: 12537667]

(66). Dijkgraaf I, John AW, Kruijtzer JAW, Liu S, Soede A, Oyen WJG, Corstens FHM, Liskamp RMJ, Boerman OC. Improved targeting of the $\alpha_v\beta_3$ integrin by multimerization of RGD peptides. Eur. J. Nucl. Med. Mol. Imaging 2007;34:267–273. [PubMed: 16909226]2007

(67). Dijkgraaf I, Liu S, Kruijtzer JAW, Soede AC, Oyen WJG, Liskamp RMJ, Corstens FHM, Boerman OC. Effect of linker variation on the in vitro and in vivo characteristics of an ^{111}In-labeled RGD Peptide. Nucl. Med. Biol 2007;34:29–35. [PubMed: 17210459]

(68). Line BR, Mitra A, Nan A, Ghandehari H. Targeting tumor angiogenesis: comparison of peptide and polymer-peptide conjugates. J. Nucl. Med 2005;46:1552–1560. [PubMed: 16157540]

(69). Beer AJ, Haubner R, Goebel M, Luderschmidt S, Spilker ME, Webster HJ, Weber WA, Schwaiger M. Biodistribution and pharmacokinetics of the $\alpha_v\beta_3$-selective tracer ^{18}F-Galacto-RGD in cancer patients. J. Nucl. Med 2005;46:1333–1341. [PubMed: 16085591]

(70). Haubner R, Weber WA, Beer AJ, Vabulience E, Reim D, Sarbia M, Becker KF, Goebel M, Hein R, Wester HJ, Kessler H, Schwaiger M. Noninvasive visuallization of the activiated $\alpha_v\beta_3$ integrin in cancer patients by positron emission tomography and [^{18}F]Galacto-RGD. PLOS Medicine 2005;2:e70, 244–252. [PubMed: 15783258]

(71). Kenny LM, Coombes RC, Oulie I, Contractor KB, Miller M, Spinks TJ, McParland B, Cohen PS, Hui A, Palmieri C, Osman S, Glaser M, Turton D, Al-Nahhas A, Aboagye EO. Phase I trial of the positron-emitting Arg-Gly-Asp (RGD) peptide radioligand ^{18}F-AH111585 in breast cancer patients. J. Nucl. Med 2008;49:879–886. [PubMed: 18483090]

(72). Shi J, Wang L, Kim YS, Zhai S, Liu Z, Chen X, Liu S. Improving tumor uptake and excretion kinetics of ^{99m}Tc-labeled cyclic Arginine-Glycine-Aspartic (RGD) dimers with triglycine linkers. J. Med. Chem 2008;51:7980–7990. [PubMed: 19049428]

(73). Wang L, Kim YS, Shi J, Zhai S, Jia B, Liu Z, Wang F, Chen X, Liu S. Improving tumor targeting capability and pharmacokinetics of ^{99m}Tc-labeled cyclic RGD dimers with PEG_4 linkers. Mol. Pharm 2009;6:231–245. [PubMed: 19067525]

(74). Anderson CJ, Green MA, Fujibayashi Y. Chemistry of copper radionuclides and radiopharmaceutical products. Handbook of Radiopharmaceuticals 2003:401–422.

(75). Blower PJ, Lewis JS, Zweit J. Copper radionuclides and radiopharmaceuticals in nuclear medicine. Nucl. Med. Biol 1996;23:957–980. [PubMed: 9004284]

(76). Reichert DE, Lewis JS, Anderson CJ. Metal complexes as diagnostic tools. Coord. Chem. Rev 1999;184:3–66.

(77). Liu S. Bifunctional coupling agents for target-specific delivery of metallic radionuclides. Advanced Drug Delivery Reviews 2008;60:1347–1370. [PubMed: 18538888]

(78). Jain RK. Transport of molecules in the tumor interstitium: a review. Cancer Res 1987;47:3039–3051. [PubMed: 3555767]

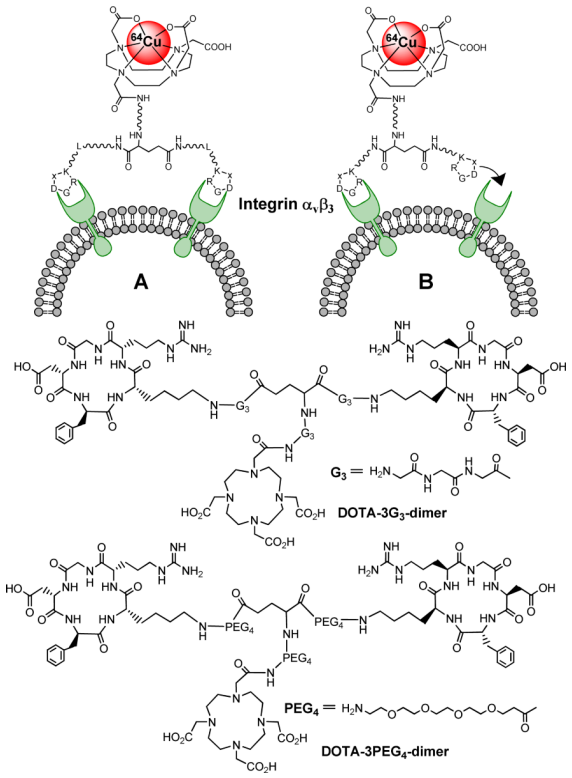

Figure 1.

Novel DOTA-conjugated cyclic RGD dimers (DOTA-3G_3-dimer and DOTA-3PEG_4-dimer) and schematic illustration of interactions between cyclic RGD dimers and integrin a_vb_3. **A**: the distance between two RGD motifs is long, and the cyclic RGD dimer is able to bind integrin $\alpha_v\beta_3$ in a "bivalent" fashion. **B**: the distance between two RGD motifs is not long enough for simultaneous integrin $\alpha_v\beta_3$ binding, but the RGD concentration is "locally enriched" in the vicinity of neighboring integrin $\alpha_v\beta_3$ once the first RGD motif is bound. In both cases, the result would be higher integrin $\alpha_v\beta_3$ binding affinity for the multimeric cyclic RGD peptides.

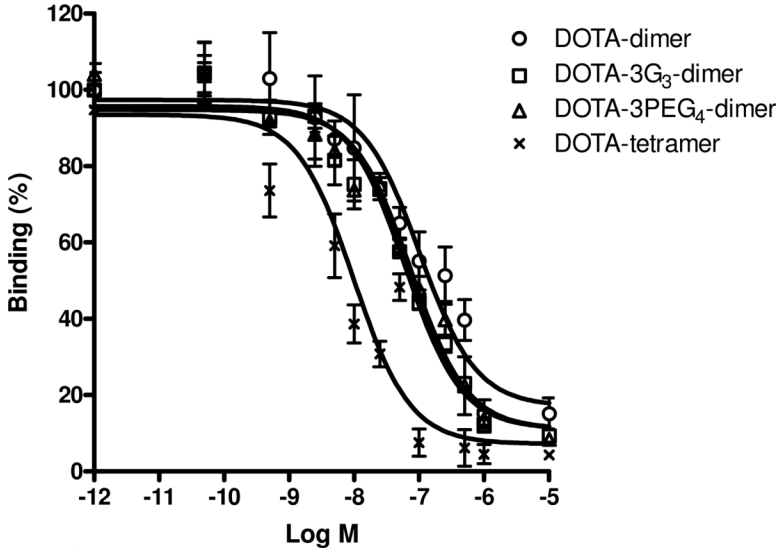

Figure 2.

In vitro inhibition of ^{125}I-echistatin bound to integrin $\alpha_v\beta_3$ on U87MG glioma cells by DOTA-dimer, DOTA-3G$_3$-dimer, DOTA-3PEG$_4$-dimer and DOTA-tetramer. Their IC$_{50}$ values were calculated to be 102 ± 5, 62 ± 6, 74 ± 3 and 10 ± 2 nM, respectively.

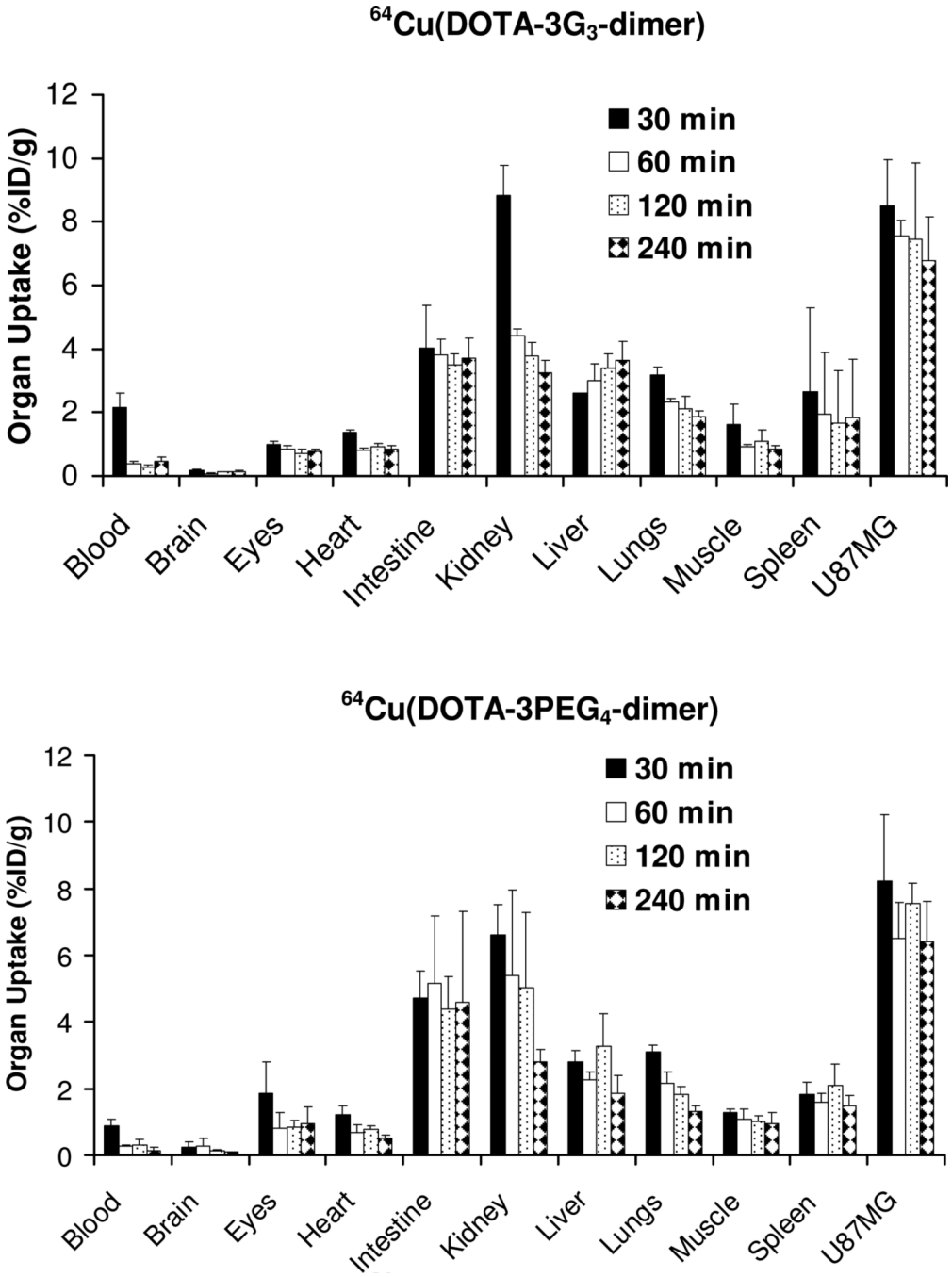

Figure 3.
Biodistribution data for ^{64}Cu(DOTA-3G$_3$-dimer) and ^{64}Cu(DOTA-3PEG$_4$-dimer) in athymic nude mice (n = 4) bearing U87MG glioma xenografts.

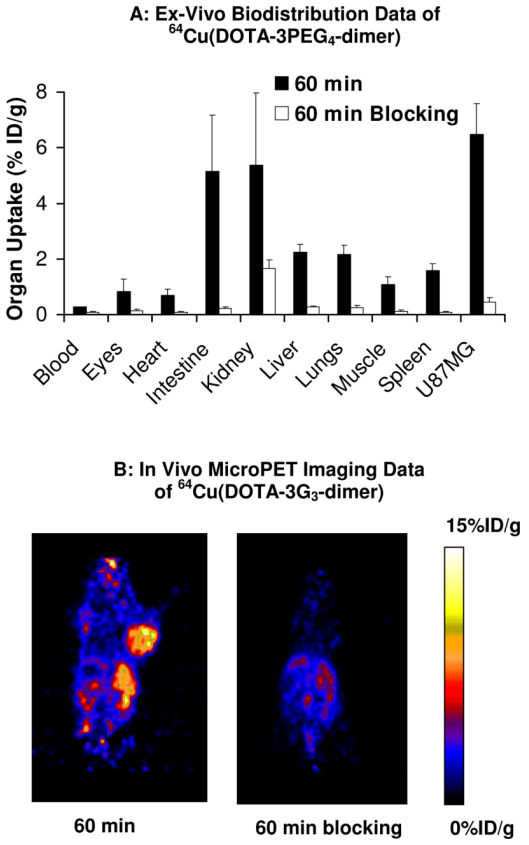

Figure 4.

Biodistribution for ^{64}Cu(DOTA-3PEG$_4$-dimer) (n = 4) and in vivo microPET imaging data for^{64}Cu(DOTA-3G$_3$-dimer) (n = 3) in athymic nude mice bearing U87MG glioma xenografts in the absence/presence of excess E[c(RGDfK)]$_2$ at 60 min p.i.

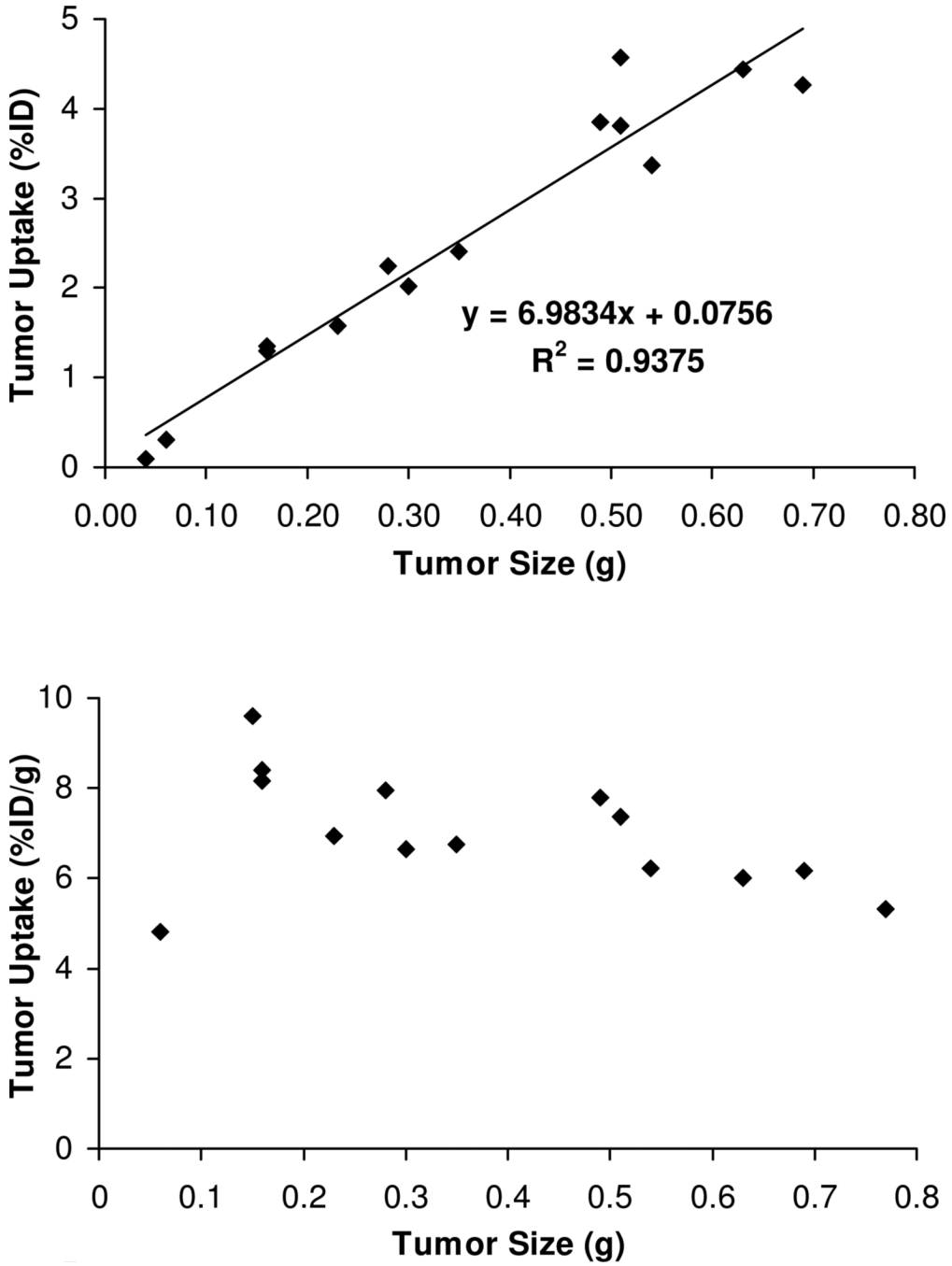

Figure 5.
The relationship between tumor size and tumor uptake for ^{64}Cu(DOTA-3PEG$_4$-dimer) at 120 min p.i. in the athymic nude mice (n = 7 with 14 tumors) bearing the U87MG glioma xenografts.

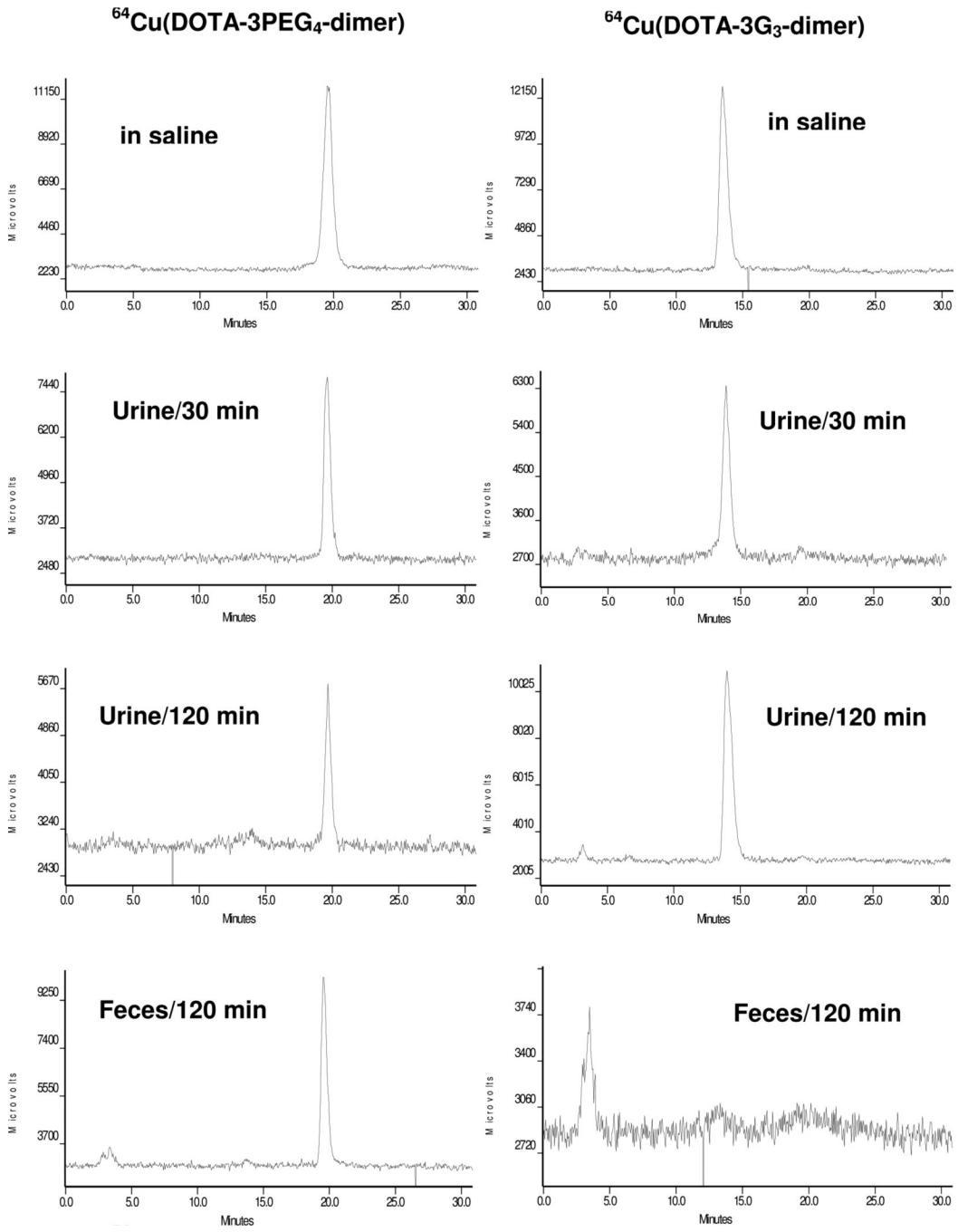

Figure 6.

Typical radio-HPLC chromatograms (Method 2) for ^{64}Cu(DOTA-3PEG$_4$-dimer) (left) and ^{64}Cu(DOTA-3G$_3$-dimer) (right) in saline before injection, in urine at 30 min and 120 min p.i., and in feces at 120 min p.i.